Inorg. Chem. **2007**, *46*, 8228–8237

Inorganic Chemistry

Article

Supramolecular Aggregation of Mononuclear Triorganophosphinegold(I) 2-Mercaptobenzamides: Solution Structures, Thermal Decomposition, and Photoluminescence

Jun-Gill Kang,[*,†] Hyung-Kook Cho,[†] Changmoon Park,[†] Sock-Sung Yun,[*,†] Jae-Kyung Kim,[‡]
Grant A. Broker,[§] Douglas R. Smyth,[⊥] and Edward R. T. Tiekink[*,§]

Department of Chemistry, Chungnam National University, Yuseong, Daejon 305-764, Republic of Korea, High Explosives Team, Agency for Defense Development (ADD), P.O. Box 35-5, Yuseong, Daejon 305-600, Republic of Korea, Department of Chemistry, The University of Texas, One UTSA Circle, San Antonio, Texas 78249-0698, Department of Chemistry, The University of Adelaide, Australia 5005

Received May 25, 2007

The crystal structures of $R_3PAu[SC_6H_4C(=O)NH_2\text{-}2]$, R = Et (**1**), Ph (**2**), and Cy (**3**) show linear coordination geometries for gold defined by sulfur and phosphorus atoms. Supramolecular aggregation via $\{\cdots H–N–C=O\}_2$ synthons lead to dimeric aggregates in each case. In (**1**) and (**2**), the aggregates are spherical, but steric effects exerted by cyclohexyl rings in (**3**) dictate a rodlike form; no Au···Au interactions were noted in the crystal structures. Solvent dependence in their NMR spectra is correlated with intra- and intermolecular hydrogen bonding. The compounds uniformly decompose under controlled conditions to give gold. The complexes excited by UV light produce strong blue-green luminescence. The configuration interaction singles (CIS) post-Hartree–Fock (HF) calculations for the compounds indicate that it is the charge transfer from the sulfur and π-orbitals of $SC_6H_4C(=O)NH_2\text{-}2$ to gold that produce the emission from gold. The assignment of the observed luminescence is presented in terms of the relaxed excited states of gold, in which the vibronic interactions for three p-orbitals of gold are taken into account.

Introduction

The structural chemistry of gold(I) compounds continues to attract significant attention because of the wide variety of supramolecular structural motifs observed in their solid-state chemistry, as well as their predilection to furnish luminescent materials: mono- and multinuclear complexes of Au(I) produce characteristic luminescence over a wide range of 350−700 nm. The rich structural diversity of gold compounds is contributed to by the possibility of the formation of attractive aurophilic interactions that are attributed to correlation and relativistic effects.[1−4] These Au···Au interactions can be significant and most important in the determination of supramolecular aggregation patterns because they are comparable in energy to hydrogen-bonding interactions.[5,6] Indeed, such considerations lead to studies investigating the competition between/complementarity of hydrogen-bonding and aurophilic interactions.[7−9] Beyond aesthetics, gold compounds are now well-known to demonstrate solid-state and solution luminescence characteristics. Accordingly, a full range of gold compounds have been

---

[*] To whom correspondence should be addressed. E-mail: jgkang@cnu.ac.kr (J.-G.K.); ssyun@cnu.ac.kr (S.-S.Y.); Edward.Tiekink@utsa.edu (E.R.T.T.).

[†] Chungnam National University.

[‡] Agency for Defense Development (ADD).

[§] The University of Texas.

[⊥] The University of Adelaide. Present address: Department of Nuclear Medicine, PET & Bone Densitometry, Royal Adelaide Hospital, South Australia 5000, Australia

(1) Schmidbaur, H. *Chem. Soc. Rev.* **1995**, *24*, 391.

(2) Pyykkö, P. *Chem. Rev.* **1997**, *97*, 597.

(3) Pyykkö, P. *Angew. Chem., Int. Ed.* **2004**, *43*, 4412.

(4) Schmidbaur, H.; Cronje, S.; Djordjevic, B.; Schuster, O. *Chem. Phys.* **2005**, *311*, 151.

(5) Schmidbaur, H. *Nature (London)* **2001**, *413*, 31.

(6) Pyykkö, P.; Runeberg, N.; Mendizabal, F. *Chem.*−*Eur. J.* **1997**, *3*, 1451.

(7) Schneider, W.; Bauer, A.; Schmidbaur, H. *Organometallics* **1996**, *15*, 5445.

(8) Hollatz, C.; Schier, A.; Riede, J.; Schmidbaur, H. *Chem. Commun.* **1999**, 111.

(9) (a) Smyth, D. R.; Vincent, B. R.; Tiekink, E. R. T. *CrystEngComm* **2000**, *2*, 115. (b) Smyth, D. R.; Vincent, B. R.; Tiekink, E. R. T. *Z. Kristallogr.* **2001**, *216*, 298.

10.1021/ic701022e CCC: $37.00

explored in this context, such as organometallic species,[10−13] thiolates,[14,15] oxo-species,[16] and mixed-metal systems, for example, with thallium[17] and silver,[18−20] where interactions between closed-shell systems are again important. Phosphinegold(I) thiolates also demonstrate luminescence,[21−24] and research into the question as to the source of these photophysical and photochemical properties is of considerable interest.[25,26] While the formation of aurophilic interactions in specialized phosphinegold(I) thiolates has been directly correlated with luminescence and has led to the development of novel analytical detection systems,[27−29] phosphinegold(I) thiolates and related systems that crystallize without Au···Au interactions can also be luminescent with their luminescence assigned to charge transfer from ligand to gold.[30−33] In connection with the above, previously, we investigated the spectroscopic properties of (*o*-tolyl)$_3$PAuCl[34] and of a series of pseudo-polymorphs of (*o*-tolyl)$_3$PAu[SC$_6$H$_4$CO$_2$H-2][31] and performed configuration interaction singles (CIS) post-Hartree−Fock (HF) calculations to model their electronic structures. The pseudo-polymorphs of (*o*-tolyl)$_3$PAu[SC$_6$H$_4$CO$_2$H-2] produced strong luminescence, peaking at 500 nm, while (*o*-tolyl)$_3$PAuCl produced weak luminescence, peaking at 450 nm. The observed luminescence of these compounds was strongly associated with S-to-Au and Cl-to-Au charge transfers, respectively. As a contribution to the delineation of the mechanisms responsible for the luminescence properties observed in mononuclear phosphinegold(I) thiolates, the series of compounds R$_3$PAu[SC$_6$H$_4$C(=O)NH$_2$-2], R = Et (**1**), Ph (**2**), and Cy (**3**), was synthesized, and their structural and optical properties were comprehensively investigated. This included the measurements of the absorption, photoluminescence, and excitation spectra. In addition, the CIS post-HF calculations on the molecular orbitals and excited states of the complexes were performed to reveal the nature of the absorbing and emitting states presented.

Experimental Section

Synthesis and Spectroscopic Characterization. The R$_3$PAu[SC$_6$H$_4$C(=O)NH$_2$-2], R = Et (**1**), Ph (**2**), and Cy (**3**), compounds were prepared in high yields from the reaction of the R$_3$PAuCl precursor and 2-mercaptobenzamide in the presence of KOH using established procedures.[35] Slow evaporation of an ethanol solution of **1** and of an acetone solution of **3** afforded suitable crystals for the X-ray study. Vapor diffusion of diethyl ether into a chloroform solution of **2** yielded suitable crystals. Melting points were routinely determined using a Gallenkamp digital melting point apparatus. Infrared spectra for all compounds were recorded as KBr discs on a Perkin-Elmer Spectrum BX FT-IR spectrophotometer in the range of 400−4000 cm^{-1}. ^{1}H (and ^{1}H−^{1}H COSY), ^{13}C, and ^{31}P{^{1}H} NMR were recorded on a Varian Gemini 2000 spectrometer operating at 300.145, 75.479, and 121.501 MHz, respectively. ^{1}H−^{13}C HSQC, HMQC, and HMBC 2-D NMR measurements were performed on a Varian INOVA NMR spectrometer operating at 599.952 and 150.873 MHz for ^{1}H and ^{13}C NMR, respectively. Spectra were measured in CDCl$_3$ or DMSO-*d*$_6$, where indicated, and referenced to TMS (85% H$_3$PO$_4$ for ^{31}P{^{1}H} NMR) or the appropriate solvent resonance. Microanalyses were performed by Chemical & Microanalytical Services Pty Ltd (CMAS), Belmont, Victoria, Australia.

Et$_3$PAu[SC$_6$H$_4$C(=O)NH$_2$-2] (1). Colorless crystals in 75% yield. Obsd (Calcd): C, 33.45 (33.41); H, 4.55 (4.53%); N, 2.91 (3.00%). IR (KBr, cm^{-1}): 1666 (s) ν(C−O); 3123 (m), 3339 (m) ν(N−H). mp: 146−148 °C. ^{13}C{^{1}H} NMR (DMSO-*d*$_6$): δ 8.9 (Cβ), 17.0 d (Cα, $^{1}J_{\mathrm{C-P}} = 33.5$ Hz), 123.0 (C5), 128.0 (C6), 128.4 (C4), 134.8 (C3), 138.5 (C1), 140.0 (C2), 170.2 (C=O). ^{31}P NMR (DMSO-*d*$_6$): δ 39.5.

Ph$_3$PAu[SC$_6$H$_4$C(=O)NH$_2$-2] (2). Colorless crystals in 89% yield. Obsd (Calcd): C, 47.64 (47.69); H, 6.30 (6.24%); N, 2.07 (2.22%). IR (KBr, cm^{-1}): 1661 (s) ν(C−O); 3114 (m), 3338 (m) ν(N−H). mp: 166−167 °C. ^{13}C{^{1}H} NMR (DMSO-*d*$_6$): δ 123.4 (C5), 128.0 (C6), 128.1 (C4), 128.9 d (Cα, $^{1}J_{\mathrm{C-P}} = 56.7$ Hz), 129.5 d (Cγ, $^{3}J_{\mathrm{C-P}} = 11.5$ Hz), 132.0 d (Cδ, $^{4}J_{\mathrm{C-P}} = 2.3$ Hz), 133.7 d (Cβ, $^{2}J_{\mathrm{C-P}} = 13.7$ Hz), 135.0 (C3), 138.3 (C1), 139.3 (C2), 170.6 (C=O). ^{31}P NMR (DMSO-*d*$_6$): δ 38.2.

Cy$_3$PAu[SC$_6$H$_4$C(=O)NH$_2$-2] (3). Yellow crystals in 94% yield. Obsd (Calcd): C, 49.13 (49.11); H, 3.43 (3.46%); N, 2.17 (2.29%). IR (KBr, cm^{-1}): 1665 (vs) ν(C−O); 3123 (m), 3305 (s) ν(N−H). mp: 200−210 °C. ^{13}C{^{1}H} NMR (CDCl$_3$): δ 25.8 (Cδ), 27.0 d (Cβ, $^{2}J_{\mathrm{C-P}} = 11.7$ Hz), 30.8 (Cγ), 33.3 d (Cα, $^{1}J_{\mathrm{C-P}} = 28.1$ Hz), 124.1 (C5), 129.4 (C4), 131.4 (C6),135.0 (C1), 136.6 (C3), 140.1 (C2), 170.1 (C=O). ^{31}P NMR (CDCl$_3$): δ 57.4.

---

(10) Chen, J.; Mohamed, A. A.; Abdou, H. E.; Bauer, J. A. Krause; Fackler, J. P., Jr.; Bruce, A. E.; Bruce, M. R. M. *Chem. Commun.* **2005**, 1575.

(11) Tang, H.-S.; Zhu, N.; Yam, V. W.-W. *Organometallics* **2007**, *26*, 22.

(12) Elbjeirami, O.; Yockel, S.; Campana, C. F.; Wilson, A. K.; Omary, M. A. *Organometallics* **2007**, *26*, 2550.

(13) Barnard, P. J.; Wedlock, L. E.; Baker, M. V.; Berners-Price, S. J.; Joyce, D. A.; Skelton, B. W.; Steer, J. H. *Angew. Chem.* **2006**, *45*, 5966.

(14) Schmidbaur, H.; Graf, W.; Müller, G. *Angew. Chem., Int. Ed. Engl.* **1988**, *27*, 417.

(15) Codina, A.; Fernández, E. J.; Jones, P. G.; Laguna, A.; López-de-Luzuriaga, J. M.; Monge, M.; Olmos, M. E.; Pérez, J.; Rodríguez, M. A. *J. Am. Chem. Soc.* **2002**, *124*, 6781.

(16) Bojan, V. R.; Fernandez, E. J.; Laguna, A.; Lopez-de-Luzuriaga, J. M.; Monge, M.; Olmos, M. E.; Silvestru, C. *J. Am. Chem. Soc.* **2005**, *127*, 11564.

(17) Fernandez, E. J.; Laguna, A.; Lopez-De-Luzuriaga, J. M.; Elena O. M.; Perez, J. *Chem. Commun.* **2003**, 1760.

(18) Catalano, V. J.; Moore, A. L. *Inorg. Chem.* **2005**, *44*, 6558.

(19) Wang, Q.-M.; Lee, Y.-A.; Crespo, O.; Deaton, J.; Tang, C.; Gysling, H. J.; Gimeno, M. C.; Larraz, C.; Villacampa, M. D.; Laguna, A.; Eisenberg, R. *J. Am. Chem. Soc.* **2004**, *126*, 9488.

(20) Colis, J. C. F.; Staples, R. J.; Tripp, C.; Labrecque, D.; Patterson, H. *J. Phys. Chem. B* **2005**, *109*, 102.

(21) Assefa, Z.; McBurnett, B. G.; Staples, R. J.; Fackler, J. P., Jr; Assmann, B.; Angermaier, K.; Schmidbaur, H. *Inorg. Chem.* **1995**, *34*, 75.

(22) Yam, V. W.-W.; Chan, C.-L.; Cheung, K.-K. *J. Chem. Soc., Dalton Trans.* **1996**, 4019.

(23) Tzeng, B.-C.; Chan, C.-K.; Cheung, K.-K.; Che, C.-M.; Peng, S.-M. *Chem. Commun.* **1997**, 135.

(24) Bardají, M.; Calhorda, M. J.; Costa, P. J.; Jones, P. G.; Laguna, A.; Reyes, Pérez, M.; Villacampa, M. D. *Inorg. Chem.* **2006**, *45*, 1059.

(25) Fung, E. Y.; Olmstead, M. M.; Vickery, J. C.; Balch, A. L. *Coord. Chem. Rev.* **1998**, *171*, 151.

(26) van Zyl, W. E.; Lopez-de-Luzuriaga, J. M.; Fackler, J. P., Jr. *J. Mol. Struct.* **2000**, *516*, 99.

(27) Yam, V. W.-W.; Chan, C.-L.; Li, C.-K. *Angew. Chem., Int. Ed.* **1998**, *37*, 2857.

(28) Yam, V. W.-W.; Cheng, E. C.-C. *Gold Bull.* **2001**, *34*, 20.

(29) Li, C.-K.; Lu, X.-X.; Wong, K. M.-C.; Chan, C.-L.; Zhu, N.; Yam, V. W.-W. *Inorg. Chem.* **2004**, *43*, 7421.

(30) Hao, L.; Mansour, M. A.; Lachicotte, R. J.; Gysling, H. J.; Eisenberg, R. *Inorg. Chem.* **2000**, *39*, 5520.

(31) Yun, S.-S.; Kim, J.-K.; Jung, J.-S.; Park, C.; Kang, J.-G.; Smyth, D. R.; Tiekink, E. R. T. *Cryst. Growth Des.* **2006**, *6*, 899.

(32) Ho, S. Y.; Cheng, E. C.-C.; Tiekink, E. R. T.; Yam, V. W.-W. *Inorg. Chem.* **2006**, *45*, 8165.

(33) Ovejero, P.; Mayoral, M. J.; Cano, M.; Lagunas, M. C. *J. Organomet. Chem.* **2007**, *692*, 1690.

(34) Kang, J.-G.; Park, C.; Tiekink, E. R. T. *Bull. Korean Chem. Soc.* **2006**, *27*, 299.

(35) Smyth, D. R.; Tiekink, E. R. T. *Z. Kristallogr. NCS* **2002**, *217*, 357.

Table 1. Crystallographic Data and Refinement Details for $R_3PAu[SC_6H_4C({=}O)NH_2\text{-}2]$, R = Et (1), Ph (2), and Cy (3)

	1	**2**	**3**
formula	$C_{13}H_{21}AuNOPS$	$C_{25}H_{21}AuNOPS$	$C_{25}H_{39}AuNOPS$
fw	467.32	611.45	629.59
cryst syst	monoclinic	triclinic	triclinic
space group	$P2_1$	$P\bar{1}$	$P\bar{1}$
a (Å)	7.995(1)	10.576(4)	11.028(2)
b (Å)	17.491(6)	11.232(4)	13.240(7)
c (Å)	11.664(1)	10.205(6)	9.756(2)
α (deg)	90	114.62(3)	106.01(3)
β (deg)	104.55(1)	90.25(4)	97.11(2)
γ (deg)	90	91.66(3)	108.65(3)
V (Å^3)	1578.8(5)	1101.4(9)	1261.8(7)
Z	4	2	2
D_c (g cm^{-3})	1.966	1.844	1.657
F(000)	896	592	628
μ(Mo Kα) (mm^{-1})	9.573	6.886	6.013
measured data	4007	5329	6100
unique data	3997	5054	5801
obsd data with $I \geq 2.0\sigma(I)$	3743	4358	4941
variables	309	271	271
R, obsd data; all data	0.027; 0.063	0.023; 0.057	0.027; 0.067
a; b in weighting scheme	0.026; 0.503	0.028; 0.730	0.035; 1.825
R_w, obsd data; all data	0.047; 0.068	0.034; 0.060	0.039; 0.071
largest residual (e Å^{-3})	1.14	0.82	1.22
CCDC no.	602447	602448	602446

X-ray Crystallography. Intensity data for **1**−**3** were measured at 173 K on a Rigaku AFC7R diffractometer fitted with Mo Kα radiation, so that θ_{max} was 27.5°. The structures were solved by heavy-atom methods.[36] Typically, refinement was on F^2,[37] using data that had been corrected for absorption effects with an empirical procedure,[38] with non-hydrogen atoms modeled with anisotropic displacement parameters, with hydrogen atoms in their calculated positions, and using a weighting scheme of the form $w = 1/[\sigma^2(F_o^2) + (aP)^2 + bP]$, where $P = (F_o^2 + 2F_c^2)/3)$. For **1**, in which two independent molecules comprise the asymmetric unit, the structure was refined as a racemic twin precluding the determination of absolute structure. One of the triethylphosphine ligands in **1** was found to be disordered, and this was resolved by modeling (isotropic refinement) the methylene-carbon atoms over two sites; from the refinement, the site occupancies were found to be equal. The maximum residual electron density peak of 1.14 e Å^{-3} in **1** was located in the vicinity of the disordered residue, and in the case of **3**, it was in the vicinity of the gold atom. Figure 2 was drawn at the 50% probability level using ORTEP,[39] Figures 3 and S2 were drawn with DIAMOND,[40] and data manipulation and analyses were performed with teXsan[41] and PLATON.[42] Crystallographic data and refinement details are given in Table 1.

Thermal Analysis. The thermal decomposition mechanisms of **1**−**3** were investigated on a TGA 50 apparatus (Mettler-Toledo GmbH, Switzerland) fitted with a standard platinum pan. The conditions of thermogravimetry (TG) were as follows: sample masses of about 1 mg were heated at a rate of 10 °C min^{-1} under a nitrogen atmosphere. The differential scanning calorimetry (DSC) experiments were carried out with a model 821^e apparatus (Mettler-Toledo GmbH, Switzerland) fitted with a standard aluminum pan. The conditions of DSC were as follows: sample masses of about 1 mg were heated at a rate of 10 °C min^{-1} under a nitrogen atmosphere. A sample of indium was used as the reference. In other experiments, the decomposition residues obtained by heating 7−8 mg of the samples in an aluminum crucible (70 μL) up to 320−330 °C under a nitrogen atmosphere were subjected to scanning electron microscopy (SEM) analysis on a model XL-30-FEG Philips microscope operating at 20 kV and WD 10 mm. For **1**−**3**, the respective phase transitions were in the ranges of 147.4−149.3−151.3, 155.3−165.3−169.2 and 202.7−206.8−209.0, and 188.1−200.7−203.8 °C. Thermal decomposition for **1** occurred in the temperature ranges of 261.3−317.7 (DSC) and 144.7−228.0−320.0 °C (DTG) resulting in 58.02% weight loss. The theoretical weight loss is 57.85% assuming that gold is the final product. The formation of gold was confirmed by SEM analysis. For **2**, the ranges were 271.1−324.8 (DSC) and 152.2−300.0−339.7 °C (DTG) with 66.78% weight loss (cf., theoretical 67.79%). For **3**, the temperature ranges were 286.1−331.9 (DSC) and 187.3−324.0−344.7 °C (DTG) with a weight loss of 68.83% (cf., 68.72% theoretical).

Optical Measurements. For luminescence and excitation spectra measurements, samples in microcrystalline or powder states were placed on the cold finger of an Oxford CF-1104 cryostat using silicon grease. Excited light from either a He−Cd laser or an Oriel 1000-W Xe arc lamp, passed through an Oriel MS257 monochromator, was focused on the sample. The luminescence spectrum was measured at a 90° angle with respect to the excitation direction with an ARC 0.5 m Czerny-Turner monochromator equipped with a cooled Hamamatsu R-933−14 photomultiplier tube. The luminescence spectra of the complexes were measured at 10 K, 78 K, and room temperature.

Results and Discussion

Syntheses and Characterization. The $Et_3PAu[SC_6H_4C({=}O)NH_2\text{-}2]$ (**1**), $Ph_3PAu[SC_6H_4C({=}O)NH_2\text{-}2]$ (**2**), and $Cy_3PAu[SC_6H_4C({=}O)NH_2\text{-}2]$ (**3**) compounds were readily synthesized from the metathetical reaction between the R_3PAuCl precursor and $HSC_6H_4C({=}O)NH_2\text{-}2$ in the presence of base. A single amide ν(C═O) band was observed in their IR spectra, with a stretching frequency in the range of 1652−1668 cm^{-1}. Two N−H absorptions were also observed with frequencies typically near 3120 and 3320 cm^{-1}. In their NMR, unambiguous assignment of the proton resonances was determined by the 2D methods of ^{1}H−^{1}H COSY, ^{1}H−^{13}C HSQC (or HMQC), and ^{1}H−^{13}C HMBC and, interestingly, showed significant solvent dependence in terms of their chemical shifts.

The doublet of doublets corresponding to H6 in $R_3PAu[SC_6H_4C({=}O)NH_2\text{-}2]$ comes into resonance at approximately 8.05 ppm in $CDCl_3$ solution but occurs at approximately 7.35 ppm in DMSO-d_6. The shift of up to 0.70 ppm suggests that the amide group undergoes a conformational flip. The chemical shift of approximately 8.05 ppm in $CDCl_3$ indicates that the H6 proton is deshielded because of anisotropy of

---

(36) Beurskens, P. T.; Admiraal, G.; Beurskens, G.; Bosman, W. P.; García-Granda, S.; Smits, J. M. M.; Smykalla, C. *The DIRDIF Program System*; Technical Report of the Crystallography Laboratory; University of Nijmegen: Nijmegen, The Netherlands, 1992.

(37) Sheldrick, G. M. *SHELXL97, Program for Crystal Structure Refinement*; University of Göttingen: Göttingen, Germany, 1997.

(38) Walker, N.; Stuart, D. *Acta Crystallogr., Sect. A* **1983**, *39*, 158.

(39) Johnson, C. K. *ORTEP*. Report ORNL-5138; Oak Ridge National Laboratory: Oak Ridge, TN 1976.

(40) *DIAMOND, Visual Crystal Structure Information System*, version 2.1e; Crystal Impact: Bonn, Germany, 2002.

(41) *teXsan: Structure Analysis Software*; Molecular Structure Corp.: The Woodlands, TX, 1997.

(42) Spek, A. L. *PLATON, A Multipurpose Crystallographic Tool*; Utrecht University: Utrecht, The Netherlands, 2006.

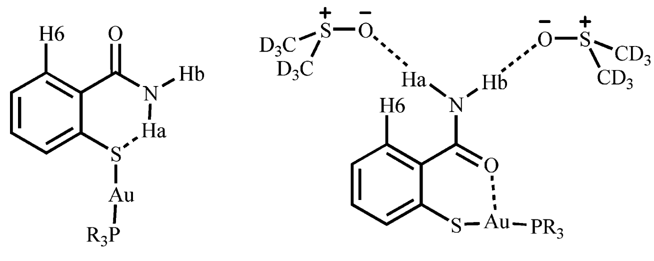

(a) $CDCl_3$ (b) d_6-DMSO

Figure 1. Proposed solution structures of $R_3PAu[SC_6H_4C({=}O)NH_2\text{-}2]$ in (a) $CDCl_3$ and (b) DMSO-d_6 solution.

the carbonyl π-bond. The proximity of the H6 proton to the carbonyl bond is the result of an intramolecular $N{-}H\cdots S$ hydrogen bond locking the amide group into that particular geometry, as shown in Figure 1a. Further evidence for the formation of an intramolecular hydrogen bond comes from the chemical shifts of the two amide protons. The proton participating in the intramolecular hydrogen bond, Ha, is deshielded and appears downfield in the range of 8.72−8.86 ppm. The second amide proton, Hb, comes into resonance near 6.0 ppm, approximately 2.7 ppm upfield from Ha. Upon titration of small aliquots of DMSO-d_6 into a $CDCl_3$ solution of $Cy_3PAu[SC_6H_4C({=}O)NH_2\text{-}2]$ (**3**), the H6 resonance progressively moves upfield as shown in Figure S1; Table S1 lists the ^1H resonances. In 100% DMSO-d_6, the amide group is orientated such that the H6 proton is removed from the deshielding zone of the carbonyl π-bond. Furthermore, the signals from the amide protons, Ha and Hb, progressively move toward each other, indicating that their chemical environments become similar in DMSO-d_6 solution. Because the spectral features of each **1** and **2** resemble those just described for **3**, it is concluded that similar structures exist for all three compounds. The proposed solution structure of $R_3PAu[SC_6H_4C({=}O)NH_2\text{-}2]$ in DMSO-d_6 solution is shown in Figure 1b, indicating intermolecular hydrogen bonds between the amide protons and the polar DMSO-d_6 solvent.

The ^{13}C and $^{31}P\{^1H\}$ chemical shifts and $^{31}P\{^1H\}{-}^{13}C$ coupling constants are consistent with compounds of this type.[43] The assignment of the aromatic thiolate ^{13}C resonances was aided by the 2D methods of $^1H{-}^{13}C$ HSQC (or HMQC) and $^1H{-}^{13}C$ HMBC and also shows some solvent dependence, but it is not as dramatic as that for the ^1H NMR.

Analogous solution behavior as just described was observed for the related $R_3PAu[SC_6H_4C({=}O)OH\text{-}2]$[43] systems and in this case, both forms similar to those shown in Figure 1 were crystallized.[44] Despite our best attempts, only one crystal form was ever isolated in the present study because of the dual hydrogen-bonding capacity of the amide functionality that always allows for the formation of intra- and intermolecular hydrogen bonding, that is, $N{-}H\cdots S$ and $N{-}H\cdots O$ interactions, respectively. In contrast, in $R_3PAu[SC_6H_4C({=}O)OH\text{-}2]$, the acidic hydrogen can form an intramolecular $O{-}H\cdots S$ interaction or an intermolecular $O{-}H\cdots O$ interaction, thereby allowing for the possibility of structural isomer formation.

Crystallography. The molecular structure of $Et_3PAu[SC_6H_4C({=}O)NH_2\text{-}2]$ (**1**) is shown in Figure 2a, and selected geometric parameters are collected in Table 2 for this and the remaining structures described herein. Two independent molecules comprise the crystallographic asymmetric unit of **1**, but these are virtually identical. Indeed, there are only minor conformational differences between the molecules, mainly associated with the phosphine ligands, in that for the first independent molecule, two of the terminal methyl groups are orientated toward the gold atom whereas the other is directed away. By contrast, for the second molecule, all three methyl groups are directed toward the gold atom. The familiar linear P−Au−S coordination geometry is observed with the Au−S bond distance being significantly longer than the Au−P bond. The magnitude of the C2−S2 bond indicates that the anion is coordinating as a thiolate ligand. There is a significant twist about the S2−C2 bond, and further, the amide residue is not coplanar with the aromatic ring as seen in the torsion angle data included in Table 2. Such a conformation most likely alleviates some of the steric pressure in this region of the molecule. This is also reflected in the significant deviations from the ideal 120° angles about the C2 atom. Relief of at least some of this steric pressure can be envisioned in a scenario where there is a twist about the C1−C7 bond that places the oxygen atom in close proximity to gold. Indeed, such interactions are well-known in phosphinegold(I) thiolate chemistry.[44−48] However, in this case, the imperative for the observed conformation is the formation of an intramolecular $N{-}H\cdots S$ interaction.[49] This leaves the remaining N−H atoms available for intermolecular interactions so that the two molecules comprising the asymmetric unit associate about a pseudo-center-of-inversion, resulting in the formation of the $\{\cdots H{-}N{-}C{=}O\}_2$ synthon as shown in Figure 2a.

The molecular structure and formation of a $\{\cdots H{-}N{-}C{=}O\}_2$ synthon is also repeated in the structure of Ph_3PAu-

---

(43) de Vos, D.; Clements, P.; Pyke, S. M.; Smyth, D. R.; Tiekink, E. R. T. *Metal-Based Drugs* **1999**, *6*, 31.

(44) Smyth, D. R.; Vincent, B. R.; Tiekink, E. R. T. *Cryst. Growth Des.* **2001**, *1*, 113.

(45) (a) Siasios, G.; Tiekink, E. R. T. *Z. Kristallogr.* **1993**, *204*, 95. (b) Siasios, G.; Tiekink, E. R. T. *Z. Kristallogr.* **1993**, *205*, 261.

(46) Römbke, P.; Schier, A.; Schmidbaur, H. *J. Chem. Soc., Dalton Trans.* **2001**, 2482.

(47) Barreiro, E.; Casas, J. S.; Couce, M. D.; Sánchez, A.; Sordo, J.; Varela, J. M.; Váquez-López, E. M. *Dalton Trans.* **2003**, 4754.

(48) Ho, S. Y.; Tiekink, E. R. T. *CrystEngComm* **2007**, *9*, 368.

(49) Geometric parameters describing selected intermolecular interactions in $R_3PAu[SC_6H_4C({=}O)NH_2\text{-}2]$, R = Et (**1**), Ph (**2**), and Cy (**3**). (**1**): $N1{-}H1a\cdots O1a$ = 1.97 Å, $N1\cdots O1a$ = 2.825(13) Å, angle at H = 163° for symmetry operation *x*, *y*, *z*; $N1{-}H1b\cdots S2$ = 2.58 Å, $N1\cdots S2$ = 3.145(9) Å, 123° (*x*, *y*, *z*); $N1a{-}H1a1\cdots O1$ = 2.02 Å, $N1a\cdots O1$ = 2.871(14) Å, 164° (*x*, *y*, *z*); $N1a{-}H1b1\cdots S2a$ = 2.56 Å, $N1a\cdots S2a$ = 3.127(10) Å, 123° (*x*, *y*, *z*); $C21a{-}H21c\cdots O1a$ = 2.51 Å, $C21a\cdots O1a$ = 3.48(3) Å, 164° (1 + *x*, *y*, *z*); $C12{-}H12a\cdots Cg(C1a{-}C6a)$ = 2.94 Å, $C12\cdots Cg(C1a{-}C6a)$ = 3.514(13) Å, 118° (−1 + *x*, *y*, −1 + *z*). (**2**) : $N1{-}H1a\cdots O1$ = 1.99 Å, $N1\cdots O1$ = 2.869(5) Å, 176° (−*x*, 1 − *y*, 1 − *z*); $N1{-}H1a\cdots S2$ = 2.53 Å, $N1\cdots S2$ = 3.118(4) Å, 125° (*x*, *y*, *z*); $C13{-}H13\cdots Cg(C21{-}C26)$ = 3.00 Å, $C13\cdots Cg(C21{-}C26)$ = 3.716(5) Å, 134° (1 − *x*, −*y*, 1 − *z*); $C34{-}H34\cdots Cg(C1{-}C6)$ = 2.91 Å, $C34\cdots Cg(C1{-}C6)$ = 3.666(5) Å, 137° (1 − *x*, −*y*, −*z*); $C5{-}H5\cdots Cg(C31{-}C36)$ = 2.84 Å, $C5\cdots Cg(C31{-}C36)$ = 3.731(6) Å, 156° (*x*, 1 + *y*, *z*). (**3**): $N1{-}H1a\cdots O1$ = 2.02 Å, $N1\cdots O1$ = 2.893(6) Å, 174° (−*x*, −1 − *y*, −1 − *z*); $N1{-}H1b\cdots S2$ = 2.25 Å, $N1{-}H1b\cdots S2$ = 3.008(4) Å, 144° (*x*, *y*, *z*).

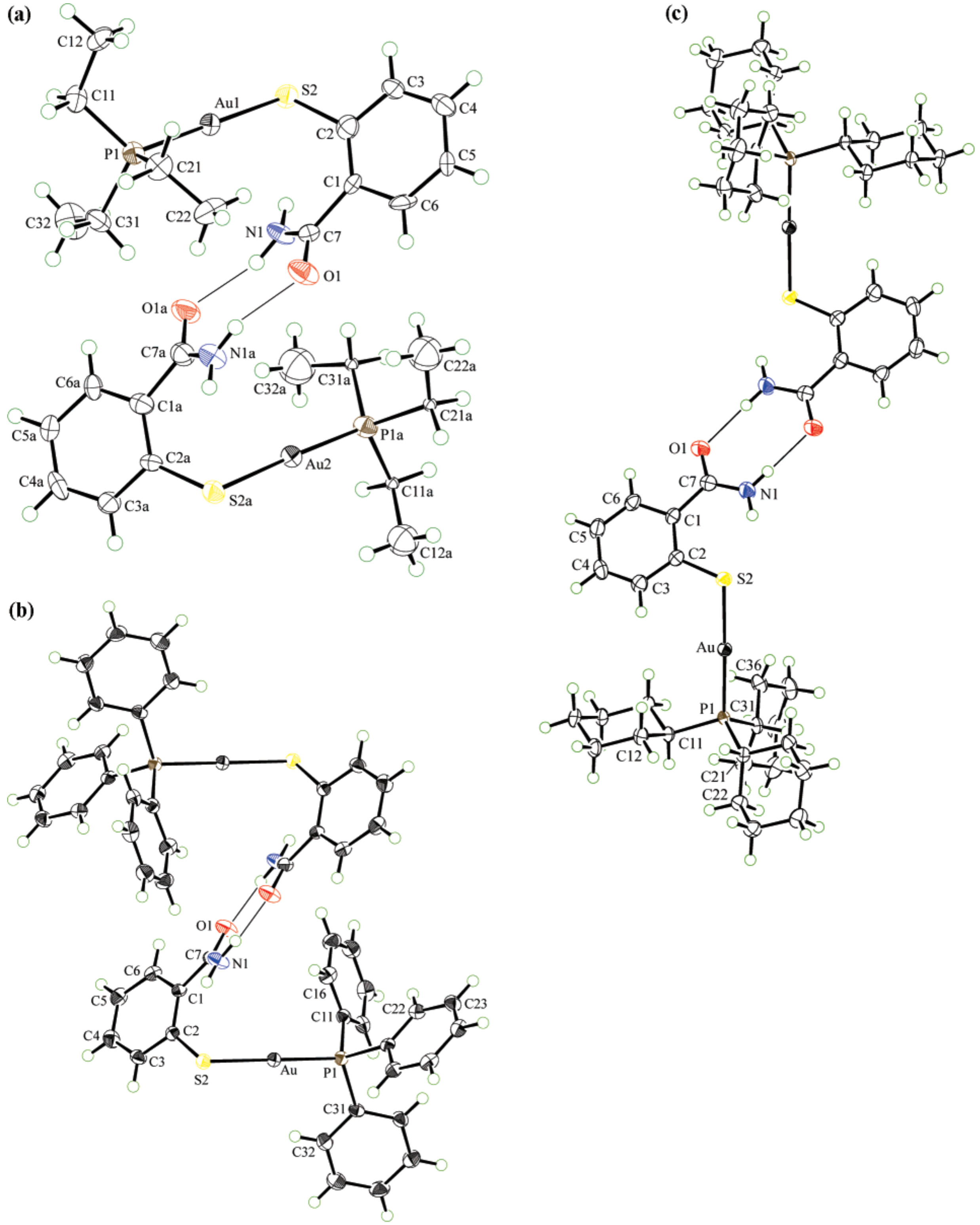

Figure 2. Molecular structures, atom-labeling scheme, and hydrogen-bonding interactions for (a) the two independent molecules of $Et_3PAu[SC_6H_4C(=O)NH_2\text{-}2]$ (**1**), (b) centrosymmetrically related molecules of $Ph_3PAu[SC_6H_4C(=O)NH_2\text{-}2]$ (**2**), and (c) centrosymmetrically related molecules of $Cy_3PAu[SC_6H_4C(=O)NH_2\text{-}2]$ (**3**).

$[SC_6H_4C(=O)NH_2\text{-}2]$ (**2**), Figure 2b. The comparable interatomic bond distances are equal within experimental error, but there is a marginally greater distortion away from the linear geometry about the gold atom in **2** compared with that in **1**. The result of the intermolecular hydrogen bonding in each of **1** and **2** is the formation of spherical aggregates.

In $Cy_3PAu[SC_6H_4C(=O)NH_2\text{-}2]$ (**3**), Figure 2c, where the coordination geometry and geometric parameters are basically equivalent to those observed in the preceding structures, the shape of the supramolecular aggregate is distinct despite the formation of the prevalent $\{\cdots H-N-C=O\}_2$ synthon. The adoption of the rod or cylinder type of arrangement in

Table 2. Selected Interatomic Parameters for $R_3PAu[SC_6H_4C(=O)NH_2\text{-}2]$, R = Et (**1**), Ph (**2**), and Cy (**3**)

	1, **1a**	**2**	**3**
Au−S2	2.315(4), 2.319(4)	2.3095(14)	2.3120(16)
Au−P1	2.262(4), 2.253(4)	2.2610(13)	2.2680(15)
S2−C2	1.780(12), 1.778(11)	1.786(4)	1.782(4)
C7−O1	1.238(13), 1.257(14)	1.233(5)	1.235(5)
C7−N1	1.316(14), 1.330(15)	1.332(5)	1.326(6)
P1−Au−S2	178.89(12), 178.23(12)	176.66(4)	178.46(4)
Au−S2−C2	102.6(4), 102.6(4)	102.91(12)	103.07(14)
C2−C1−C6	120.0(11), 120.5(11)	118.9(3)	118.4(4)
C2−C1−C7	126.6(10), 125.1(11)	126.4(3)	127.9(4)
C6−C1−C7	113.3(10), 114.4(11)	114.6(3)	113.7(4)
O1−C7−N1	123.0(10), 121.9(11)	122.4(4)	121.1(4)
O1−C7−C1	119.5(10), 119.1(11)	119.9(4)	119.2(4)
N1−C7−C1	117.5(10), 119.0(11)	117.6(3)	119.7(4)
Au/S2/*C*2/C1	−128.1(9), 123.7(8)	−60.2(3)	−140.8(4)
*C*2/C1/C7/O1	−147.7(12), 147.9(12)	151.8(4)	174.7(5)
*C*2/C1/C7/N1	35.7(16), −34.6(18)	−32.6(6)	−6.1(8)

3 is dictated by steric considerations, as have been discussed in closely related $R_3PAu(S_2COR')$, R = alkyl or aryl,[46,47] and $Cy_3PAu(SC_6H_4CO_2H\text{-}2)$[44] systems. Put simply, if the hydrogen-bonded dimer in **3** adopts the same conformation as seen in each of **1** and **2**, there would be impossible steric interactions between the cyclohexyl rings. Thus, while the $\{\cdots H{-}N{-}C{=}O\}_2$ synthon persists, the shape of the aggregate is rodlike. In terms of molecular geometry, the more-open arrangement allows the amide moiety to be effectively coplanar with the remaining portion of the thiolate ligand.

The dimeric aggregates in **1** associate to form a chain as shown in Figure 3a. The primary mode of association between the molecules of **1** is interactions of the type C−H$\cdots$O that extend in the *a*-direction.[49] Chains are linked via C−H$\cdots\pi$ interactions involving the C12-H atom and the ring centroid of (C1a-C6a)^{i}. The net result of the aforementioned contacts is a layer arrangement running parallel to (101). The dimeric aggregates in **2** also associate into a chain along (011), but this time via Au$\cdots$S2^{i} interactions of 3.345(2) Å between centrosymmetrically related molecules (symmetry: i −*x*, −*y*, −*z*).[49] Chains are linked into layers via 6-fold phenyl embraces;[50,51] the Ph_3P group has an approximate rotor conformation: the Au−P1−C_{ispo}−C torsion angles are 17.0(4), 48.4(4), and 54.6(4)° for the C32, C16, and C26 rings, respectively, and the P$\cdots$P distance is 6.85 Å. Additional C−H$\cdots\pi$ interactions involving the mercaptobenzoate ring also stabilize the structure.[49] The well-defined supramolecular aggregation patterns operating in the crystal structures of both **1** and **2** is somewhat lacking in the crystal structure of **3**. As indicated by the crystal packing diagram shown in Figure S2, molecules stack into columns along the *c*-direction to form rows of gold atoms. However, there are no Au$\cdots$Au interactions of note, and in the absence of hydrogen bonding, C−H$\cdots\pi$, and $\pi\cdots\pi$ interactions, the crystal packing is best described as being stabilized by hydrophobic interactions between interdigitated dimeric aggregates.

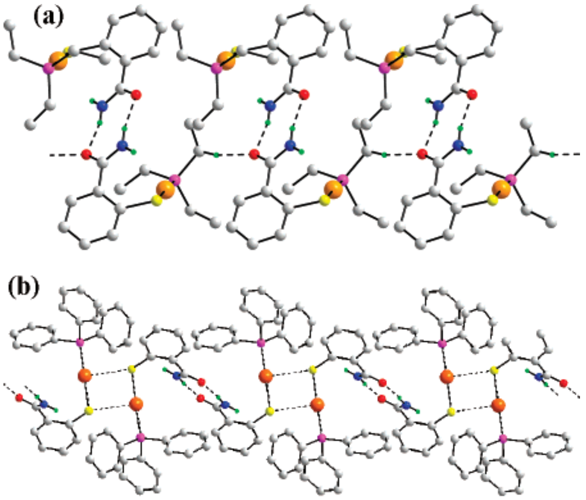

Figure 3. (a) Chain mediated by C−H$\cdots$O interactions in the structure of $Et_3PAu[SC_6H_4C(=O)NH_2\text{-}2]$ (**1**). (b) Chain mediated by Au$\cdots$S interactions in the structure of $Ph_3PAu[SC_6H_4C(=O)NH_2\text{-}2]$ (**2**). For clarity, only hydrogen atoms involved in hydrogen-bonding interactions are shown.

Table 3. Electronic Absorption Data (Recorded in CH_2Cl_2 Solution) for $HSC_6H_4C(=O)NH_2\text{-}2$, Ph_3P, $Et_3PAu[SC_6H_4C(=O)NH_2\text{-}2]$ (**1**), $Ph_3PAu[SC_6H_4C(=O)NH_2\text{-}2]$ (**2**), and $Cy_3PAu[SC_6H_4C(=O)NH_2\text{-}2]$ (**3**)

	λ/nm ($\epsilon \times 10^{-3}$/M^{-1} cm^{-1})
$HSC_6H_4C(=)NH_2\text{-}2$	305(0.2), 246(0.4), 203(0.1)
Ph_3P	286(0.3), 247(0.4), 190(0.1)
1	323 sh (2.2), 282 sh (5.4), 230 (12.6)
2	319 sh (3.6), 291 sh (6.1), 237 (33.1)
3	323 sh (2.5), 282 sh (5.9), 230 (13.3)

Spectroscopic Properties. Absorption and Reflectance. The absorption spectra of the uncoordinated $HSC_6H_4C(=O)NH_2\text{-}2$ and Ph_3P molecules and of $Et_3PAu[SC_6H_4C(=O)NH_2\text{-}2]$ (**1**), $Ph_3PAu[SC_6H_4C(=O)NH_2\text{-}2]$ (**2**), and $Cy_3PAu[SC_6H_4C(=O)NH_2\text{-}2]$ (**3**), all dissolved in CH_2Cl_2, were measured in the 225−600 nm range (Table 3). As shown in Figure 4a, the absorption spectra of **1** and **3** are almost identical with three absorption bands appearing at 323, 282, and 230 nm. Hereafter, these bands are referred to as A, B, and C absorption bands in order of increasing energy. The intensities of the A and B absorption bands were very weak, compared with that of the C absorption band. The absorption spectrum of **2** is slightly different with the three absorption bands appearing at 319, 291, and 237 nm but with the C-absorption band being significantly more intense than those of the others. The reflectance spectra of the uncoordinated $[HSC_6H_4C(=O)NH_2\text{-}2]$ and Ph_3P molecules and of **1**−**3** were also measured in the powdered state (see Table 4). As shown in Figure 4b, the reflectance spectrum of **2** is very different from those of **1** and **3**. For the latter, the reflectance spectrum showed less well-defined band shapes, compared with the absorption spectrum measured in solution. Assuming that the peak position of the solution state was blue-shifted by approximately 110 nm, the positions of the A, B, and C absorption bands of the powdered state were indicated by arrows in the reflectance spectrum (see Figure 4b).

PL and Excitation Spectra. The PL spectrum of $Et_3PAu[SC_6H_4C(=O)NH_2\text{-}2]$ (**1**) in the solid-state was measured at 10 K, 78 K, and room temperature (RT). As shown in Figure 5a, whereas **1** had significant luminescence intensity at 78.8 K, at RT, the intensity was markedly decreased. There were no remarkable differences in the spectral shapes measured

---

(50) Scudder, M.; Dance, I. *J. Chem. Soc., Dalton Trans* **1998**, 329.
(51) Scudder, M.; Dance, I. *J. Chem. Soc., Dalton Trans* **1998**, 3167.

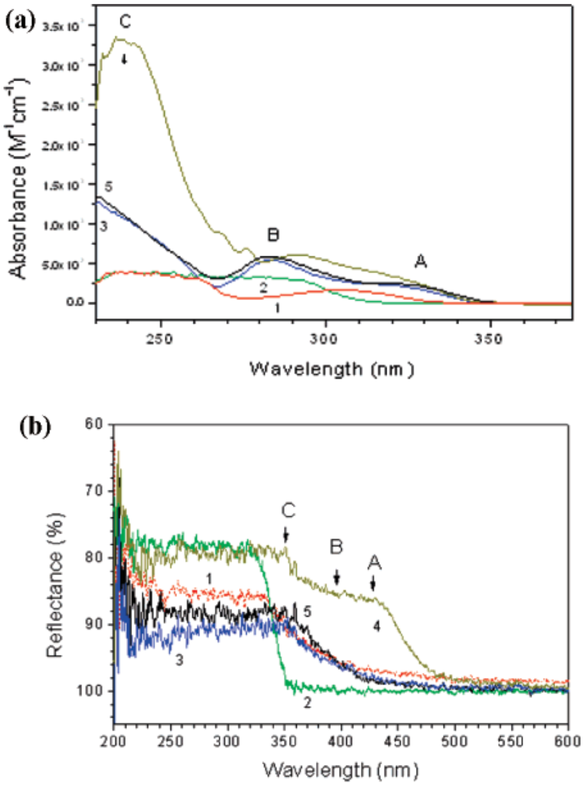

Figure 4. (a) Absorption (measured in CH_2Cl_2 solution) and (b) reflection spectra of spectrum 1, $HSC_6H_4C({=}O)NH_2$-2; 2, Ph_3P; 3, $Et_3PAu[SC_6H_4C({=}O)NH_2$-2]; 4, $Ph_3PAu[SC_6H_4C({=}O)NH_2$-2]; and 5, $Cy_3PAu[SC_6H_4C({=}O)NH_2$-2].

Table 4. Emission and Excitation Data $Et_3PAu[SC_6H_4C({=}O)NH_2$-2] (**1**), $Ph_3PAu[SC_6H_4C({=}O)NH_2$-2] (**2**), and $Cy_3PAu[SC_6H_4C({=}O)NH_2$-2] (**3**) in the Powdered State at $T = 10$ K[a]

	excitation	emission
1	324 (vb), 356 (p)	503 (p), 563 (sh)
2	321 (vb), 356 (p)	492 (p), 545 (sh)
3	310 (vb), 365 (m), 440 (p)	457 (m), 503 (p), 556 (sh)

[a] vb = very broad, p = peak, sh = shoulder, m = medium.

at the three temperatures. The PL spectrum resolved into two Gaussian components, peaking at 500 and 566 nm, respectively. The 500 nm band is a main emission component (hereafter, referred to as ME). The excitation spectra of these two components were also measured at 10 K. As shown in Figure 5b, a sharpened 350 nm peak appeared with a weak 400 nm peak and a broad band as a high-energy shoulder. The 350 nm peak corresponds to the C absorption band, and the weak 400 nm band could be the B absorption. Data are summarized in Table 4.

The spectral features of $Ph_3PAu[SC_6H_4C({=}O)NH_2$-2] (**2**) are very similar to those of **1**, but the bands are blue-shifted, see Figure 5c and d. The PL spectrum was also resolved into two components: the 483 nm band as ME and a weak and broad 545 nm band as a shoulder. As shown in Figure 5d, the excitation spectra of these two components measured at 10 K are also very similar to those of **1**. The excitation spectrum of the main emission comprises a sharpened component at 356 nm and a high-energy shoulder.

In contrast to the above, the PL spectral shape of $Cy_3PAu[SC_6H_4C({=}O)NH_2$-2] (**3**) is very different and is dependent on temperature, as shown in Figure 5e. At 78 K, the PL spectrum is well resolved into three main Gaussian components, peaking at 457, 503, and 556 nm. The high-energy component, which did not appear or appeared as only a trace for **1** and **2**, gained in intensity to form the observed band. The excitation spectra of the three emissions were also measured at 78 K. As shown in Figure 5f, the excitation spectrum of ME is significantly different from those of **1** and **2**. Not only did the 350 nm band appear as a main excitation band but also the 450 nm band. The ME and low-energy emission bands were produced strongly by the 450 nm excitation, while the high-energy band was produced by the 350 nm excitation. The 450 nm excitation corresponds to the A absorption band. The series of the bands are ascribed to the vibronic distortion.

Molecular Orbitals and Electronic Transitions. The main objective of the theoretical investigation was to model the electronic structures and to determine the properties of luminescence. On the basis of the X-ray data, the molecular orbitals (MOs) and the electronic structures of **1**−**3** were calculated at the HF level[52] (see Tables S2−S4). The electronic transitions were calculated with the ZINDO semiempirical method from Gaussian 03.[52] The results for some low-lying excited states and the oscillator strengths of the three complexes are listed in Table S5−S7, respectively.

For **1**−**3**, the combinations of the π-orbital of the benzene ring and the nonbonding p-orbitals of the sulfur, oxygen, and nitrogen atoms resulted in the HOMOs. The first HOMO, h1, comprises one-nodal π-bonding orbital from the benzene ring and the p-orbitals of the sulfur atom, each with different parity, forming the antibonding character between the benzene ring and the sulfur atom. The contributions of the benzene ring and the sulfur atom were almost equal. The h2 HOMO was composed largely of another one-nodal π-bonding orbital of the benzene ring as a main part, as well as a contribution from the nonbonding p-orbitals of the oxygen, nitrogen, and sulfur atoms. With h1, three additional HOMOs were formed by the combination of the π-orbital of the benzene ring and the nonbonding p-orbitals of the sulfur. For **2**, several low-energy HOMOs correspond to the π-orbitals of the benzene rings in Ph_3P. Minor contributions from the π-orbitals of Ph_3P were also made to some low-

---

(52) Frisch, M. J.; Trucks, G. W.; Schlegel, H. B.; Scuseria, G. E.; Robb, M. A.; Cheeseman, J. R.; Montgomery, J. A., Jr.; Vreven, T.; Kudin, K. N.; Burant, J. C.; Millam, J. M.; Iyengar, S. S.; Tomasi, J.; Barone, V.; Mennucci, B.; Cossi, M.; Scalmani, G.; Rega, N.; Petersson, G. A.; Nakatsuji, H.; Hada, M.; Ehara, M.; Toyota, K.; Fukuda, R.; Hasegawa, J.; Ishida, M.; Nakajima, T.; Honda, Y.; Kitao, O.; Nakai, H.; Klene, M.; Li, X.; Knox, J. E.; Hratchian, H. P.; Cross, J. B.; Bakken, V.; Adamo, C.; Jaramillo, J.; Gomperts, R.; Stratmann, R. E.; Yazyev, O.; Austin, A. J.; Cammi, R.; Pomelli, C.; Ochterski, J. W.; Ayala, P. Y.; Morokuma, K.; Voth, G. A.; Salvador, P.; Dannenberg, J. J.; Zakrzewski, V. G.; Dapprich, S.; Daniels, A. D.; Strain, M. C.; Farkas, O.; Malick, D. K.; Rabuck, A. D.; Raghavachari, K.; Foresman, J. B.; Ortiz, J. V.; Cui, Q.; Baboul, A. G.; Clifford, S.; Cioslowski, J.; Stefanov, B. B.; Liu, G.; Liashenko, A.; Piskorz, P.; Komaromi, I.; Martin, R. L.; Fox, D. J.; Keith, T.; Al-Laham, M. A.; Peng, C. Y.; Nanayakkara, A.; Challacombe, M.; Gill, P. M. W.; Johnson, B.; Chen, W.; Wong, M. W.; Gonzalez, C.; Pople, J. A. *Gaussian 03*, revision C.02; Gaussian, Inc.: Wallingford, CT, 2004.

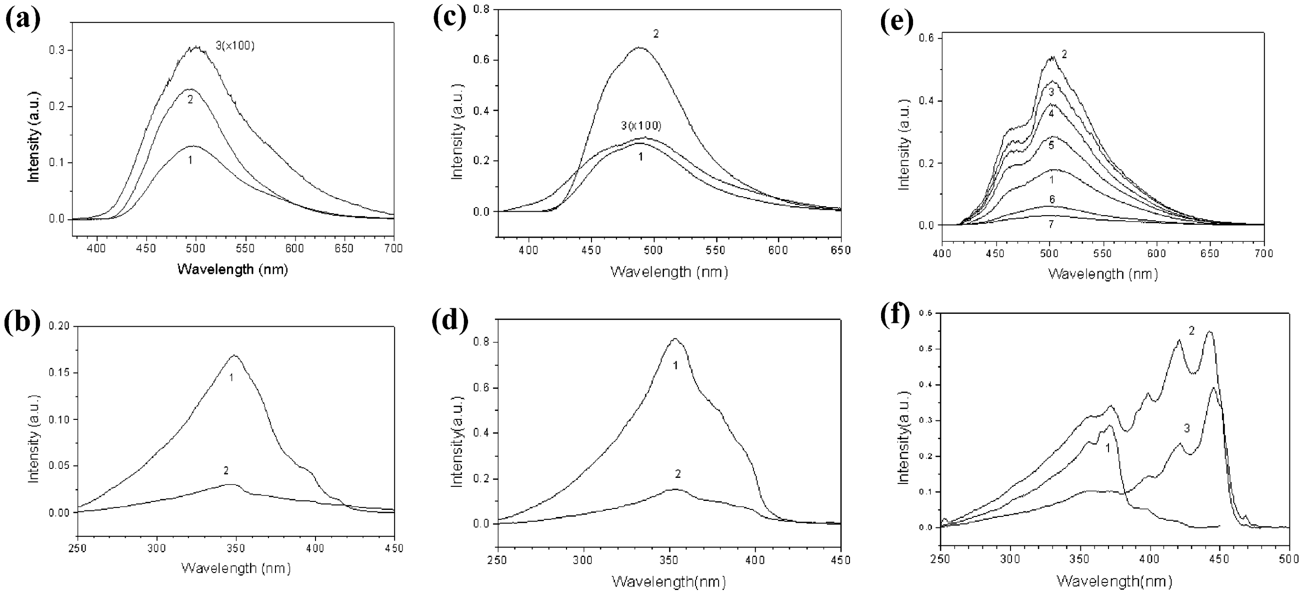

Figure 5. (a) PL at $T = 10$ K (spectrum 1), 78 K (2), and RT (3) and (b) excitation at $T = 10$ K: $\lambda_{\text{ems}} = 497$ (spectrum 1) and 585 nm (2) spectra of $Et_3PAu[SC_6H_4C(=O)NH_2\text{-}2]$ (**1**). (c) PL at $T = 10$ K (spectrum 1), 78 K (2), and RT (3) and (d) excitation at $T = 10$ K: $\lambda_{\text{ems}} = 490$ (spectrum 1) and 573 nm (2) spectra of $Ph_3PAu[SC_6H_4C(=O)NH_2\text{-}2]$ (**2**);. (e) PL at $T = 10$ K (spectrum 1), 50 (2), 78 (3), 100 (4), 120 (5), 140 (6), and 160 K (7) and (f) excitation at $T = 10$ K: $\lambda_{\text{ems}} = 470$ (spectrum 1), 503 (2), and 574 nm (3) spectra of $Cy_3PAu[SC_6H_4C(=O)NH_2\text{-}2]$ (**3**).

energy HOMOs of mercaptobenzamide. The first two lowest unoccupied molecular orbitals (LUMOs) correspond to the empty p_z- and p_y-orbitals of the gold atom, nearly perpendicular to the S−Au−P molecular axis. For **1** and **2**, the l1 LUMO is composed of the p_z of gold as the main component with the p_x-orbital as a minor component, while the l2 LUMO is composed of the p_y of the gold atom as the main component. For **3**, the l1 LUMO is composed of not only the p_z- and p_x-orbitals but also the p_y-orbital of gold with the contribution of the p_z-orbital the greatest and the p_x-orbital the least. The l2 is characterized by the linear combination of the p_y- and p_z-orbitals of gold. For **1** and **3**, the next several LUMOs were filled by the π^*-bonds of benzene ring of amide and the p-orbitals of sulfur with minor contributions from gold. For **3**, the next several LUMOs correspond primarily to the π^*-orbitals of the benzene ring in the triphenylphosphine moiety. The π^*-orbitals of the benzene ring in the mercaptobenzamide moiety appear at slightly higher energy levels. The electron density isocontours of the HOMOs and LUMOs of the Au(I) complexes are shown in Figure 6.

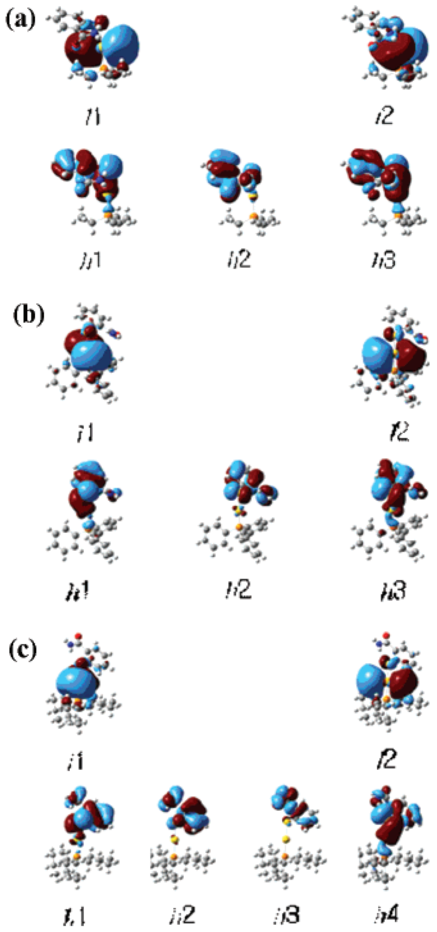

Figure 6. Contour plots of the highest- and lowest-energy molecular orbitals for (a) $Et_3PAu[SC_6H_4C(=O)NH_2\text{-}2]$ (**1**), (b) $Ph_3PAu[SC_6H_4C(=O)NH_2\text{-}2]$ (**2**), and (c) $Cy_3PAu[SC_6H_4C(=O)NH_2\text{-}2]$ (**3**).

The simulated absorption spectra of a single, gas-phase molecules produced three distinguishable bands (see Figure S3). If one assumes that there is a 120 nm red-shift for the liquid phase, those bands are in agreement with the observed A, B, and C absorption of the liquid phase. The calculated excited states (listed in Tables S5−S7) can be also classified to three groups, and these groups are responsible for the A, B, and C absorption bands, respectively. For **1** and **2**, the first four excited states (1A−4A) are involved in the A absorption band. The first 1A excited state corresponded to the intraligand transitions of the amide group. However, the oscillator strength of the transition from the ground state to 1A is almost negligible. The 2A, 3A, and 4A states arose from the h1,h3 → l1 or h1 → l2 transitions. For the A band, the transition from the X ground state to the 4A excited state is predominant, compared with the transitions to the 2A and

3A. According to the atomic charges determined from the Mulliken population analysis, for the X → 4A transition of **1**, the changes of the atomic charges of gold, sulfur, and carbon atoms of the benzene ring are +0.61, −0.30, and −0.12, respectively. For the X → 4A transition of **2**, the charge of gold was increased by 0.62, while the charges of sulfur and the benzene ring were decreased by 0.29 and 0.11, respectively. This result indicated that the A-absorption band was associated with electronic transitions of the lone-pair electrons of sulfur to gold as a main part and π-electrons of benzene ring to gold as a minor. In contrast with the cases of **1** and **2**, the 4A excited-state of **3** is not close to the 3A state but rather to the 5A state (see Figure S3c), so that the 4A excited state is involved in the B absorption band. For **3**, the X → 3A transitions with $f = 0.124$ is predominant and responsible for the A absorption band. This transition corresponds to the h1 → l2 charge transfer from sulfur to gold. For the B band of **1**, two transitions were found to be predominant with $f = 0.136$ and 0.216, respectively (see Table S5). Both of these two excited states arose mainly from the h6 and h7 to l1 transitions. Here, the h7 HOMO was contributed from s- and d-orbitals of gold (57%) and the lone-pair electrons of phosphorus (31%). The changes in the atomic charges of gold, sulfur, and the π-orbital of the benzene ring are 0.42, −0.12, and −0.12, respectively, for the former transition, and 0.55, −0.13, and −0.15, respectively, for the latter transition. Although the contribution of phosphorus to h7 is large, the changes of the atomic charge of phosphorus for the two transitions are −0.04 and −0.08, respectively. Accordingly, the B absorption band can be attributed primarily to the charge transfers to gold from sulfur and the benzene ring and to a lesser extent from phosphorus and oxygen. Similarly, for **2** and **3**, the largest transition probability in the B-absorption band was found in the charge-transfer transition. For the C-band, several transitions have relatively large probabilities. For **1**, the transition with the largest probability of $f = 0.895$ was associated with the $\pi \rightarrow \pi^*$ transitions of benzene ring as a main part and the charge transfer from sulfur to gold as a minor part. For this transition, the charges of gold and sulfur were changed by 0.17 and −0.16, respectively. The transition with the second largest oscillator strength of $f = 0.244$ corresponds to the charge transfer from the sulfur atom and the benzene ring to gold. The changes in the atomic charges of gold, sulfur, and the π-orbital of benzene ring are 0.49, −0.11, and −0.10, respectively. Accordingly, the C absorption band can be characterized by the $\pi \rightarrow \pi^*$ transitions of benzene ring mainly with the charge transfers. In contrast with **1** and **3**, complex **2** has other π-electron systems, that is, in Ph_3P. The charge transfers from the Ph_3P moieties to gold were also found to contribute the transition probabilities to the C-absorption band.

Assignment of Luminescence. Given that the observed luminescence of the complexes was produced by the charge transfer from the sulfur and the π-orbitals of the mercaptobenzamide moiety to the first two LUMOs of each complex, the A-band excited states is responsible for the observed luminescence: 2A−4A for **1** and **2** and 2A−3A for **3**. These excited states is associated with the l1 and l2 LUMOs, composed of the three p-orbitals of gold. Therefore, the observed spectral features can be interpreted in terms of the relaxed excited states (RESs) of Au(I). The vibronic interactions (VIs) are very important in understanding electronic spectra if they are of suitable magnitude. The linear vibronic interaction, known as the dynamic Jahn−Teller effect (JTE), can be estimated from the observed excitation and luminescence spectra. Because the dynamic JT energy, E_{JT}, is half the Stoke's shift, E_{JT} is 4290 cm^{-1} for **1**, 2600 cm^{-1} for **2**, and 1810 cm^{-1} for **3**. These strong JTE values indicated that the RESs of Au(I) can be formulated in terms of the vibronic interactions.

For **1** and **2**, the l1-orbital is the linear combination of the p_x- and p_z-orbitals, and the l2-orbital is predominantly the p_y-orbital of gold. The 2A and 4A excited states adapt the l1-orbital in the main, and the 3A adapts l2. Here, the energy gap between the 3A and the 4A states is only 0.04 eV, indicating that these two states are nearly degenerate. The VI of the 2-fold electronic states coupling to the bending mode (known as the Renner−Teller effect) is of primary importance for three-atom linear molecules. Upon bending, the VI can lead to splitting of the 2-fold states into symmetric A′ state as a lower level and antisymmetric A″ electronic state as a higher level, respectively, with respect to reflection in the molecular plane (*xz*). As shown in Figure 6a and b, the l1 and l2 MOs are symmetric and antisymmetric, respectively, with respect to the reflection. Accordingly, the 4A state becomes A′ and the 3A state A″. For **1** and **2**, upon the C-band excitation the A′(4A) level gains the population mainly via the nonradiative relaxation and produces the strong ME, while the lowest A′(2A) level produces the weak luminescence as the low-energy shoulder.

For **3**, the l1 and l2 orbitals, containing the p_y component are perpendicular to the molecular plane, as shown in Figure 6c. The VI coupling to the bending mode can lead the 2A and 3A excited states to two A″ RESs. The energy gap between the 2A and 3A is 0.29 eV, indicating that these two levels separated from each other. Accordingly, the A″(2A) and A″(3A) RESs are responsible for the weak low-energy and the main luminescence, respectively. The 457 nm high-energy luminescence of **3**, which was not observed for the other two complexes, could be associated with the 4A excited state. This state arose from the charge transfer from sulfur (h4) to Au (l1) and the energy gap between this state and the 3A state is ∼1.0 eV. The A″(4A) parabola could be apparently separated from the A″(3A) parabola and may give rise to the high-energy band with the characteristic band shape observed for **3**.

Acknowledgment. We gratefully acknowledge The University of Adelaide for a Postgraduate Research Award (D.R.S.) and the Australian Research Council for support of the X-ray facility. We thank Mr. Phil Clements for expert assistance with some of the 2D NMR experiments. This thermal decomposition work was supported by KOSEF research project R01-2001-00055. J.G.K. and H.K.C. acknowledge Alti-electronic Co. for financial support.

Supporting Information Available: Crystallographic information files for structures **1**−**3**, tables of ^{1}H NMR data, calculated HF molecular orbitals, and CI excited states with high oscillator strength and predominant transitions for **1**−**3**, and figures showing solvent dependence of ^{1}H spectra for **3**, unit cell diagram for **3**, and simulated absorption spectra for single gas-phase molecules of **1**−**3**. This material is available free of charge via the Internet at http://pubs.acs.org.

IC701022E